



# Substituent effects on the photophysical and electrochemical properties of iridium(III) complexes containing an arylcarbazolyl moiety



Chun Liu\*, Xiaofeng Rao, Xin Lv, Jieshan Qiu, Zilin Jin

State Key Laboratory of Fine Chemicals, Dalian University of Technology, Linggong Road 2, Dalian 116024, China

## ARTICLE INFO

### Article history:

Received 11 December 2013

Received in revised form

18 April 2014

Accepted 25 April 2014

Available online 9 May 2014

### Keywords:

Iridium complex

Carbazole

Phosphorescent material

OLEDs

Substituent effect

Ligand-free Suzuki reaction

## ABSTRACT

A series of new heteroleptic cyclometalated iridium(III) complexes containing a 9-(4-(pyridin-2-yl)phenyl)-9H-carbazole molecular framework have been successfully synthesized and characterized. All of the iridium(III) complexes are thermally stable solids and highly efficient electrophosphors. Different substituents, electron-donating group ( $-\text{CH}_3$ ) and electron-withdrawing groups ( $-\text{F}$ ,  $-\text{CF}_3$ ), were introduced into either the 4- or 5-position of the pyridyl ring in the ligands to verify their influence on the photophysical, electrochemical, photo- and electrophosphorescence properties of these iridium phosphors. Electrophosphorescent OLEDs with outstanding device performance can be fabricated based on the complex bearing a 5- $\text{CF}_3$  unit which exhibited a maximum luminance efficiency of approximately  $43.2 \text{ cd A}^{-1}$ , corresponding to an external quantum efficiency of approximately 12.6% and a power efficiency of  $27.1 \text{ lm W}^{-1}$ .

© 2014 Elsevier Ltd. All rights reserved.

## 1. Introduction

Organic light-emitting diodes (OLEDs) have attracted increasing interest in both the scientific and industrial fields due to their applications in high-resolution, multicolor displays and solid-state lighting [1–3]. In particular, phosphorescent metal complexes have been the main focus because they can harvest both singlet and triplet excitons when electrons and holes recombine, reaching up to 100% internal quantum efficiency [4]. Generally, luminescent complexes are based on heavy metals such as copper(I) [5], ruthenium(II) [6], osmium(II) [7], platinum(II) [8], or iridium(III) [9,10]. Among them, compounds based on iridium are regarded as the most promising phosphors for organic light-emitting devices, owing to their relatively short excited-state lifetime, high emission quantum yield, high photo- and thermal stability, and flexible color tuning through ligand-structure control [11,12]. To date, research on iridium complexes has focused on the design of new cyclometalating ligands either to tune the emission color of the resulting complexes or to achieve high-efficiency emission for OLEDs. In general, both the ligand framework and the substituents thereon combine to determine the optical and electronic parameters and

even the electro-luminescence performance of the resultant iridium complexes [13–16]. In other words, for both homoleptic and heteroleptic iridium complexes, the chemical structure of the cyclometalating ligand is usually the fundamental aspect to determine the emission energy and quantum efficiency of the iridium complexes. In most cases, the cyclometalating ligands are involved in the lowest-energy triplet excited state, either the ligand-centered transition or the metal-to-ligand-charge-transfer (MLCT) triplet state, which is responsible for the phosphorescence. At the same time, the structure of the ligand and even the position of the functional group on the ligand framework play important roles in tuning these physical parameters and in the electroluminescent (EL) behavior [17–21].

Up to now, among the green-emitting iridium complexes,  $\text{Ir}(\text{ppy})_2(\text{acac})$  ( $\text{ppy} = 2\text{-phenylpyridine}$ ) is one of the most important examples [11,22,23]. To improve the charge injection and transport in  $\text{Ir}(\text{ppy})_2(\text{acac})$ , the incorporation of the bulky and hole-transporting carbazole group, as a core part in the ligand frame in the iridium complexes, is anticipated to help to reduce the energy barrier height for hole injection and to decrease the triplet–triplet annihilation [24–28]. Recently, our group reported that a carbazole group could be easily incorporated as a substituent in the phenyl ring of the ppy-type ligand [29]. Since the carbazole group is a strong electron-donating group, the incorporation modifies the

\* Corresponding author. Tel.: +86 411 84986182.

E-mail address: [chunliu70@yahoo.com](mailto:chunliu70@yahoo.com) (C. Liu).

HOMO and/or the LUMO level, as well as the  $^3\text{MLCT}$  state of the complex.

Although iridium phosphors and carbazole derivatives have been widely investigated in the OLEDs area either as dopants or host materials [30,31], a systematic investigation of the substituent at the pyridyl ring on the luminescent properties of (ppy-carbazole) $_2\text{Ir}(\text{acac})$  derivatives is still absent. Herein, we report a systematic study on the synthesis and properties of a series of (ppy-carbazole) $_2\text{Ir}(\text{acac})$  derivatives. Our interest is to reveal how these simple functional groups in the pyridyl ring affect the photo-physical and electroluminescent properties of the corresponding iridium complexes. It is experimentally observed that the incorporation of substituent such as 4- $\text{CH}_3$ , 5- $\text{CH}_3$  or 5- $\text{F}$  group on the pyridyl ring of the ligand does not change significantly the phosphorescence energy and the emission color of the iridium complexes, while the introduction of a strongly electron-withdrawing 5- $\text{CF}_3$  group on the pyridyl ring of the ligand results in a great bathochromic shift of the emission color of the iridium complex.

## 2. Experimental

### 2.1. General procedures

All reagents and solvents were obtained from Alfa Aesar or Avocado, and the solvents were treated as required prior to use. Other chemicals were purchased from commercial sources and used without further purification, unless otherwise noted.  $^1\text{H}$  NMR and  $^{13}\text{C}$  NMR spectra were recorded on a 400 MHz Varian Unity Inova spectrophotometer. Mass spectra were taken on MALDI micro MX and HP1100LC/MSD MS spectrometers. The intensities of the crystal data were collected on a Bruker SMART APEX CCD diffractometer with graphite-monochromated Mo- $\text{K}\alpha$  ( $\lambda = 0.71073 \text{ \AA}$ ) using the SMART and SAINT programs. Thermogravimetry analyses (TGA) were carried out using a Perkin-Elmer thermogravimetry analyses (TGA) at a heating rate of  $10 \text{ }^\circ\text{C min}^{-1}$  under a nitrogen atmosphere. IR spectra were recorded on an FTIR NEXUS Spectrometer using KBr disks and wave numbers were given in  $\text{cm}^{-1}$ . The photoluminescence and UV–vis absorption spectra measurements were performed on a Perkin-Elmer LS55 spectrometer and a Perkin-Elmer Lambda 35 spectrophotometer, respectively. Phosphorescence lifetimes were measured on an Edinburgh FLS920 Spectrometer in degassed  $\text{CH}_2\text{Cl}_2$  solutions with excitation wavelength at 410 nm. The electrochemical measurements of these iridium complexes were carried out by using a conventional three-electrode configuration and an electrochemical workstation (BAS100B, USA) at a scan rate of  $100 \text{ mV s}^{-1}$ . A glass carbon working electrode, a Pt-wire counter electrode, and a saturated calomel electrode (SCE) reference electrode were used. All measurements were made at room temperature on samples dissolved in  $\text{CH}_2\text{Cl}_2$ , with  $0.1 \text{ M Bu}_4\text{NPF}_6$  as the electrolyte. Density functional theory (DFT) calculations using the B3LYP functional were performed. The basis set used for C, H, O, N and F atoms was 6-31G while LanL2DZ basis set were employed for iridium atoms. All these calculations were performed with Gaussian 09.

### 2.2. Preparation of materials

#### 2.2.1. Synthesis of ligands L-1–L-5 [29]

A mixture of the *N*-heteroaryl halide (1.0 mmol), 4-(9*H*-carbazol-9-yl)-phenylboronic acid (1.5 mmol),  $\text{K}_2\text{CO}_3$  (2.0 mmol),  $\text{Pd}(\text{OAc})_2$  (1.5 mol%), ethanol (6 mL) and distilled water (2 mL) was stirred at  $80 \text{ }^\circ\text{C}$  in air for indicated time (<30 min). The reaction was monitored by TLC. The reaction mixture was added to brine (30 mL) and extracted four times with ethyl acetate ( $4 \times 30 \text{ mL}$ ). The solvent

was concentrated under vacuum, and the product was isolated by short-column chromatography on silica gel (200–300 mesh).

**L-2:** yield 90%, light yellow solid.  $^1\text{H}$  NMR (400 MHz,  $\text{CDCl}_3$ ,  $25 \text{ }^\circ\text{C}$ ):  $\delta = 8.61$  (d,  $J = 4.8 \text{ Hz}$ , 1H), 8.22 (d,  $J = 8.4 \text{ Hz}$ , 2H), 8.15 (d,  $J = 8.0 \text{ Hz}$ , 2H), 7.67 (t,  $J = 8.8 \text{ Hz}$ , 3H), 7.48 (d,  $J = 8.0 \text{ Hz}$ , 2H), 7.42 (t,  $J = 7.6 \text{ Hz}$ , 2H), 7.28 (d,  $J = 7.2 \text{ Hz}$ , 2H), 7.13 (d,  $J = 4.8 \text{ Hz}$ , 1H), 2.47 (s, 3H) ppm.  $^{13}\text{C}$  NMR (100 MHz,  $\text{CDCl}_3$ ,  $25 \text{ }^\circ\text{C}$ ):  $\delta = 156.59$ , 149.72, 148.20, 140.87, 138.66, 138.37, 128.59, 127.30, 126.16, 123.61, 121.73, 120.48, 120.19, 110.00 21.49 ppm. MS (EI):  $m/z = 334.1474 [\text{M}]^+$

**L-5:** yield 96%, yellow solid.  $^1\text{H}$  NMR (400 MHz,  $\text{CDCl}_3$ ,  $25 \text{ }^\circ\text{C}$ ):  $\delta = 9.01$  (s, 1H), 8.29 (d,  $J = 8.8 \text{ Hz}$ , 2H), 8.16 (d,  $J = 7.6 \text{ Hz}$ , 2H), 8.06 (d,  $J = 6.8 \text{ Hz}$ , 1H), 7.95 (d,  $J = 8.4 \text{ Hz}$ , 1H), 7.74 (d,  $J = 8.4 \text{ Hz}$ , 2H), 7.50 (d,  $J = 8.0 \text{ Hz}$ , 2H), 7.44 (t,  $J = 7.2 \text{ Hz}$ , 2H), 7.32 (t,  $J = 7.2 \text{ Hz}$ , 2H) ppm.  $^{13}\text{C}$  NMR (100 MHz,  $\text{CDCl}_3$ ,  $25 \text{ }^\circ\text{C}$ ):  $\delta = 159.73$ , 146.83, 140.55, 139.48, 136.74, 134.20, 128.83, 127.29, 126.11, 124.93, 123.64, 120.43, 120.29, 119.95, 109.81 ppm. MS (EI):  $m/z = 388.1191 [\text{M}]^+$

#### 2.2.2. Synthesis of iridium complexes Ir-1–Ir-5

$\text{IrCl}_3 \cdot 3\text{H}_2\text{O}$  (1 mmol) and the ligands L-1–L-5 (2.5 mmol) were added to a mixture of 2-ethoxyethanol and water ( $v/v = 3:1$ , 12 mL). The mixture was refluxed under nitrogen for 24 h. Upon cooling to room temperature, the yellow precipitate was collected by filtration and washed with water. The wet solid was completely dried to give the crude chloro-bridged dimer complex. Without further purification, this dimer was added to a mixture of  $\text{K}_2\text{CO}_3$  (690 mg, 5 mmol), acetyl acetone (2 mmol), and 2-ethoxyethane (10 mL). After refluxing under nitrogen for 24 h, the solution was cooled to room temperature. The crude product was purified by column chromatography over silica using a  $\text{CH}_2\text{Cl}_2:n\text{-hexane}$  (1:1) as eluent to yield the pure product of the desired iridium complex.

**Ir-1:** yield 39%, yellow solid.  $^1\text{H}$  NMR (400 MHz,  $\text{CDCl}_3$ ,  $25 \text{ }^\circ\text{C}$ ):  $\delta = 8.50$  (d,  $J = 4.8 \text{ Hz}$ , 2H), 8.02 (d,  $J = 7.6 \text{ Hz}$ , 4H), 7.88–7.83 (m, 4H), 7.65–7.61 (m, 2H), 7.30–7.25 (m, 6H), 7.20–7.17 (m, 6H), 7.15–7.12 (m, 2H), 7.06 (d,  $J = 6.8 \text{ Hz}$ , 2H), 6.46 (d,  $J = 2.0 \text{ Hz}$ , 2H), 5.34 (s, 1H), 1.88 (s, 6H) ppm.  $^{13}\text{C}$  NMR (100 MHz,  $\text{CDCl}_3$ ,  $25 \text{ }^\circ\text{C}$ )  $\delta = 184.92$ , 167.63, 148.63, 148.26, 143.72, 140.36, 137.57, 137.37, 130.78, 125.51, 124.80, 123.19, 121.71, 119.91, 119.51, 118.70, 118.67, 110.51, 100.79, 28.88 ppm. IR (solid,  $\text{cm}^{-1}$ ): 3412, 3044, 2860, 1605, 1577, 1514, 1450, 1397, 1334, 1261, 1334, 1229, 959, 918, 776, 749, 723, 647, 616. MALDI-TOF-MS ( $m/z$ ): 930.2491 [ $\text{M}]^+$ , 831.2092 [ $\text{M-acac}]^+$ .

**Ir-2:** yield 45%, yellow solid.  $^1\text{H}$  NMR (400 MHz,  $\text{CDCl}_3$ ,  $25 \text{ }^\circ\text{C}$ ):  $\delta = 8.31$  (d,  $J = 5.6 \text{ Hz}$ , 2H), 8.02 (d,  $J = 7.6 \text{ Hz}$ , 4H), 7.80 (d,  $J = 8.0 \text{ Hz}$ , 2H), 7.66 (s, 2H), 7.29–7.25 (m, 6H), 7.19–7.16 (m, 6H), 7.12–7.09 (m, 2H), 6.88 (d,  $J = 6.0 \text{ Hz}$ , 2H), 6.46 (d,  $J = 2.0 \text{ Hz}$ , 2H), 5.31 (s, 1H), 2.45 (s, 6H), 1.87 (s, 6H) ppm.  $^{13}\text{C}$  NMR (100 MHz,  $\text{CDCl}_3$ ,  $25 \text{ }^\circ\text{C}$ )  $\delta = 184.75$ , 167.03, 148.83, 148.71, 147.64, 143.99, 140.49, 137.32, 131.03, 125.48, 124.51, 123.14, 122.84, 119.83, 119.50, 119.42, 118.54, 110.61, 100.64, 28.86, 21.37 ppm. IR (solid,  $\text{cm}^{-1}$ ): 3432, 3059, 2921, 2852, 1619, 1578, 1514, 1477, 1450, 1397, 1352, 1335, 1311, 1229, 1173, 1121, 919, 813, 750, 724, 648. MALDI-TOF-MS ( $m/z$ ): 959.2899 [ $\text{M}]^+$ , 859.2281 [ $\text{M-acac}]^+$ .

**Ir-3:** yield 26%, yellow solid.  $^1\text{H}$  NMR (400 MHz,  $\text{CDCl}_3$ ,  $25 \text{ }^\circ\text{C}$ ):  $\delta = 8.31$  (s, 2H), 8.02 (d,  $J = 8.0 \text{ Hz}$ , 4H), 7.81–7.74 (m, 4H), 7.43 (d,  $J = 8.4 \text{ Hz}$ , 2H), 7.29–7.25 (m, 6H), 7.19–7.15 (m, 6H), 7.12–7.09 (m, 2H), 6.41 (d,  $J = 6.0 \text{ Hz}$ , 2H), 5.34 (s, 1H), 2.31 (s, 6H), 1.90 (s, 6H) ppm.  $^{13}\text{C}$  NMR (100 MHz,  $\text{CDCl}_3$ ,  $25 \text{ }^\circ\text{C}$ )  $\delta = 184.80$ , 164.91, 148.02, 147.80, 143.99, 140.38, 138.17, 137.03, 131.54, 130.77, 125.44, 124.22, 123.12, 119.86, 119.42, 118.53, 118.24, 110.54, 100.79, 28.96, 18.51 ppm. IR (solid,  $\text{cm}^{-1}$ ): 3436, 3050, 3954, 1578, 1514, 1487, 1450, 1399, 1334, 1313, 1230, 1016, 811, 749, 723, 680. MALDI-TOF-MS ( $m/z$ ): 958.2781 [ $\text{M}]^+$ , 859.2336 [ $\text{M-acac}]^+$ .

**Ir-4:** yield 40%, yellow solid.  $^1\text{H}$  NMR (400 MHz,  $\text{CDCl}_3$ ,  $25 \text{ }^\circ\text{C}$ ):  $\delta = 8.39$  (m, 2H), 8.03 (d,  $J = 8.0 \text{ Hz}$ , 4H), 7.89–7.85 (m, 2H), 7.79 (t,  $J = 8.8 \text{ Hz}$ , 2H), 7.51–7.47 (m, 2H), 7.31–7.16 (m, 14H), 6.46 (d,  $J = 2.8 \text{ Hz}$ , 2H), 5.41 (s, 1H), 1.90 (s, 6H) ppm.  $^{13}\text{C}$  NMR (100 MHz,

$\text{CDCl}_3$ , 25 °C)  $\delta$  = 185.55, 147.49, 142.84, 140.22, 139.99, 137.52, 136.71, 130.25, 127.66, 125.77, 125.64, 125.30, 125.11, 124.81, 123.37, 123.26, 119.96, 119.76, 118.92, 110.14, 100.83, 28.36 ppm. IR (solid,  $\text{cm}^{-1}$ ): 3483, 3050, 2966, 1578, 1515, 1484, 1450, 1395, 1332, 1234, 1174, 859, 810, 784, 749, 722, 680, 592. MALDI-TOF-MS ( $m/z$ ): 966.2284  $[\text{M}]^+$ , 867.2361  $[\text{M-acac}]^+$ .

**Ir-5:** yield 52%, orange solid.  $^1\text{H}$  NMR (400 MHz,  $\text{CDCl}_3$ , 25 °C):  $\delta$  = 8.80 (s, 2H), 8.03 (d,  $J$  = 8.0 Hz, 4H), 7.93 (d,  $J$  = 8.4 Hz, 2H), 7.87–7.84 (m, 4H), 7.29–7.25 (m, 8H), 7.22–7.18 (m, 6H), 6.48 (d,  $J$  = 2.0 Hz, 2H), 5.39 (s, 1H), 1.93 (s, 6H) ppm.  $^{13}\text{C}$  NMR (100 MHz,  $\text{CDCl}_3$ , 25 °C)  $\delta$  = 185.78, 171.01, 150.47, 145.28, 141.64, 140.08, 139.00, 134.64, 130.70, 126.52, 125.71, 124.53, 123.44, 120.06, 119.94, 119.19, 118.44, 110.26, 101.15, 28.66 ppm. IR (solid,  $\text{cm}^{-1}$ ): 3429, 3065, 1616, 1578, 1488, 1446, 1396, 1331, 1265, 1138, 1087, 919, 815, 750, 723, 673. MALDI-TOF-MS ( $m/z$ ): 1065.2180  $[\text{M-H}]^+$ , 965.1568  $[\text{M-acac}]^+$ .

### 2.3. OLEDs fabrication and measurements

The pre-cleaned ITO glass substrates ( $30 \Omega \cdot \text{sq}^{-1}$ ) were treated by UV-ozone for 20 min. Then, a 40 nm thick NPB (4,4'-bis[*N*-(1-naphthyl)-*N*-phenylamino]-biphenyl) was deposited on the ITO glass substrates. The emitting layers were then deposited by co-evaporation of the iridium complex phosphor and the CBP (4,4'-*N,N'*-dicarbazolebiphenyl) host. Successively, TPBI (1,3,5-tris[*N*-(phenyl)-benzimidazole]benzene), LiF and Al were evaporated at a base pressure less than  $10^{-6}$  torr. The EL spectra, CIE coordinates and current–voltage–luminance characteristics of the devices were measured with a PR705 photometer and a source-measure-unit Keithley236 under ambient conditions. The forward viewing external quantum efficiency ( $\eta_{\text{ext}}$ ) was calculated using the luminance efficiency, EL spectra and human photopic sensitivity.

## 3. Results and discussion

### 3.1. Synthesis and characterization

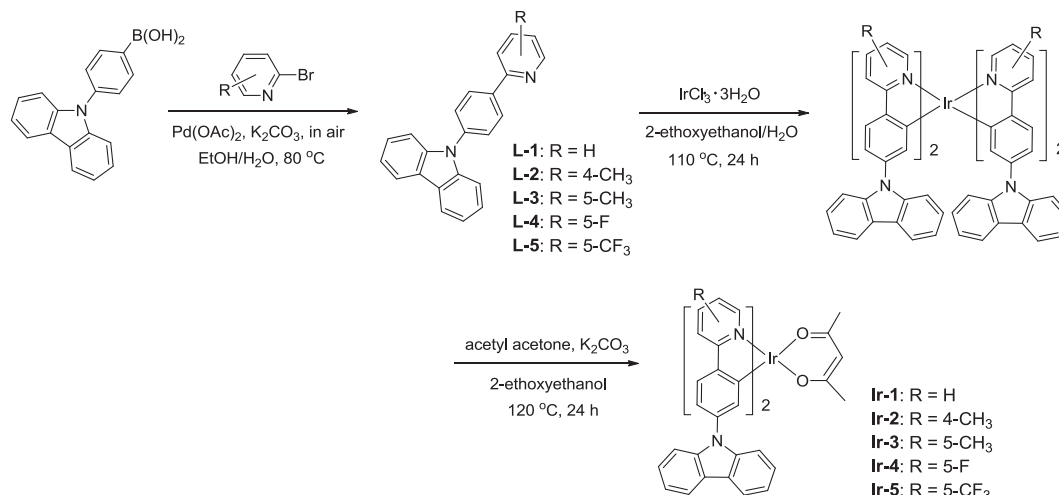
Chemical structures and the detailed synthetic protocols of these new iridium(III) complexes are shown in Scheme 1. The 9-(4-bromophenyl)carbazole was synthesized from carbazole as the starting material by a modified Ullman reaction and the 4-(9*H*-carbazol-9-yl)phenylboronic acid was synthesized in a similar procedure to that described previously [32]. As the key

compounds, the organic cyclometalating ligands were prepared by a palladium-catalyzed Suzuki reaction of 4-(9*H*-carbazol-9-yl)-phenylboronic acid with the appropriate aryl halides in aqueous ethanol under ligand-free, aerobic conditions in high yields of over 90% [29]. Our method provides a much higher yield than earlier reported traditional convergent strategies [33,34]. All of the heteroleptic complexes were synthesized through the traditional two-step procedure [35]. First, the cyclometalation of the  $\text{IrCl}_3 \cdot 3\text{H}_2\text{O}$  with each cyclometalating ligand generated the corresponding chloro-bridged dimer  $[\text{Ir}(\text{CN})_2\text{Cl}]_2$ . Then the target heteroleptic iridium(III) complexes **Ir-1**–**Ir-5** were obtained by refluxing the corresponding chloro-bridged dimer with acetyl acetone (acac) in 2-ethoxyethanol in the presence of  $\text{K}_2\text{CO}_3$ . These new complexes all exhibited good solubility and were sufficiently stable in common organic solvents such as dichloromethane, enabling them to be purified by column chromatography on silica gel.

All the ligands and complexes were fully characterized by NMR spectroscopy and MALDI-TOF mass spectrometry. Due to the characteristic singlet resonance peaks located at 5.34 and 1.88 ppm in the  $^1\text{H}$  NMR spectrum and 100.79 and 28.88 ppm in the  $^{13}\text{C}$  NMR spectrum the presence of the auxiliary acac in **Ir-1** was indicated. In each case, the MALDI-TOF mass spectrum reveals the respective parent ion peak clearly. Furthermore, crystal structures of **Ir-1** and **Ir-4** have been obtained by single crystal X-ray diffraction analyses, which provide insight on intermolecular interactions in the solid state and can also present valuable data for the computational studies of the ground-state electronic properties of the molecule. Perspective drawings of **Ir-1** and **Ir-4** are shown in Fig. 1. As confirmed by X-ray crystallography, each of the molecular structures reveals the central iridium atom to be coordinated by two anionic CN ligands and one chelating acac anion. Under a nitrogen atmosphere, the thermal properties of these iridium(III) complexes were characterized by thermogravimetric analysis (TGA), and the results are summarized in Table 1. The TGA data reveal that all the complexes have excellent thermal stability and their 5% weight-reduction temperatures ( $\Delta T_{5\%}$ ) range from 367 to 385 °C, which are necessary for high-performance OLEDs.

### 3.2. Photophysical properties

The absorption and photoluminescence (PL) spectra of all the iridium(III) complexes in  $\text{CH}_2\text{Cl}_2$  solutions are depicted in Fig. 2 and the data are summarized in Table 1. Similar UV–vis electronic



**Scheme 1.** Synthetic routes to the cyclometalated iridium(III) complexes **Ir-1**–**Ir-5**.

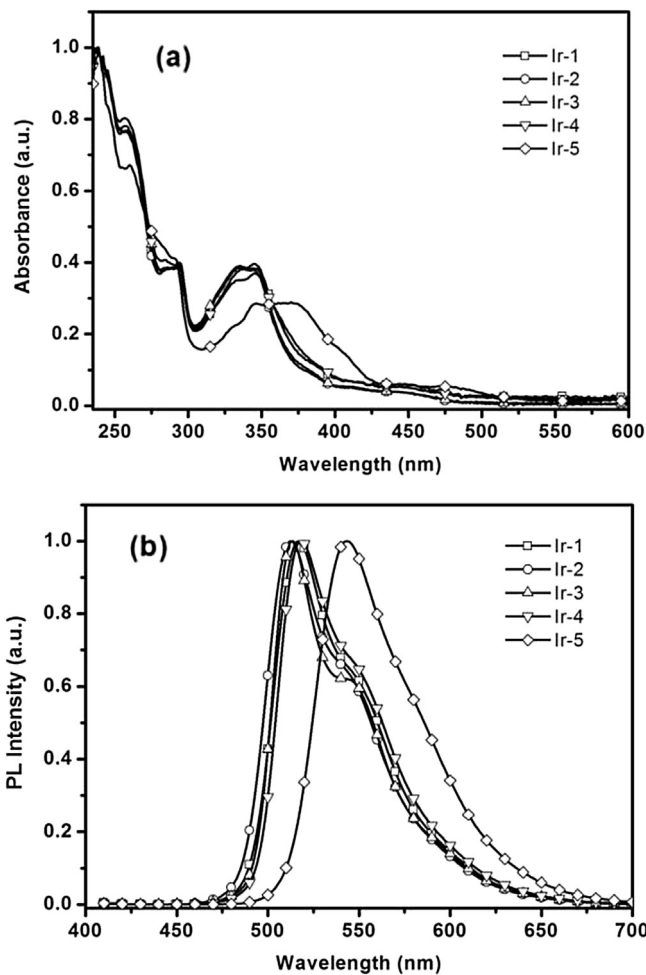
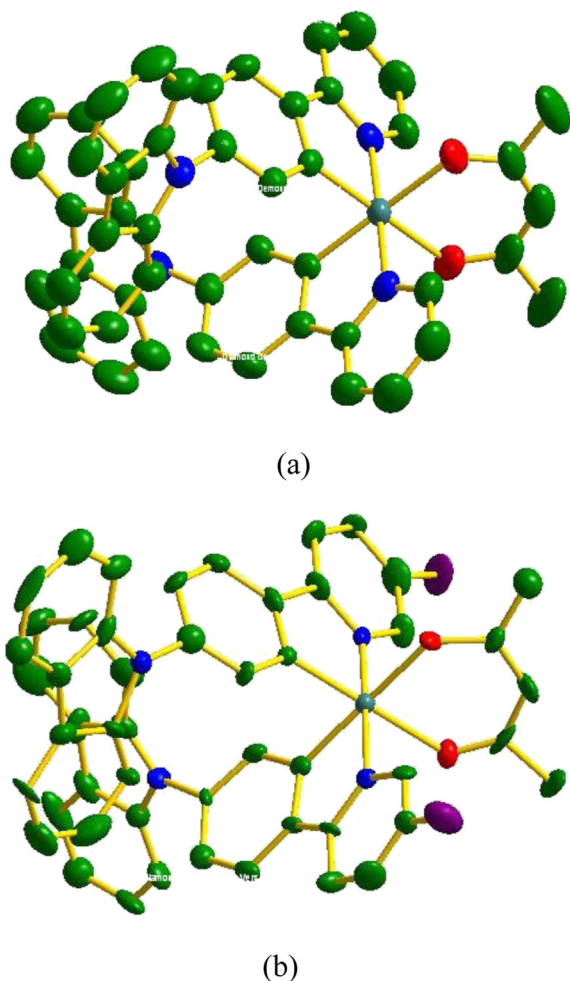


**Fig. 1.** Crystal structure of **Ir-1** (a) and **Ir-4** (b) with thermal ellipsoids drawn at 30% probability level. Labels on carbon atoms (except for those bonded to the Ir center) and hydrogen atoms are omitted for clarity.

**Fig. 2.** Absorption spectra (a) and photoluminescence spectra (b) for the iridium(III) complexes **Ir-1–Ir-5** in  $\text{CH}_2\text{Cl}_2$  at 293 K.

absorption spectra was exhibited by complexes **Ir-1–Ir-4**. In common with most iridium(III) complexes, **Ir-1–Ir-5** show two major absorption bands in their UV–vis absorption spectra. The intense bands in the ultraviolet region (below 400 nm) are assigned to the spin-allowed intraligand  $^1\pi-\pi^*$  transitions, which closely resemble the spectra of the free ligands. The next lower energy in the shoulder region of  $^1\pi-\pi^*$  transitions and the weak broad shoulders extending into the visible region (400–500 nm) with appreciable intensity are likely due to metal-to-ligand charge-transfer ( $^1\text{MLCT}$ ), spin-orbit coupling enhanced  $^3\pi-\pi^*$ , and spin-forbidden ( $^3\text{MLCT}$ ) transitions.

Upon photoexcitation at 400 nm at room temperature, complexes **Ir-1–Ir-4** show similar photoluminescence with emission peak at 513–519 nm, while the complex **Ir-5** is a yellow–green emitting with a peak at 543 nm, exhibiting a red shift 25 nm relative to **Ir-1**. Evidently, the incorporation of electron-withdrawing group (5- $\text{CF}_3$ ) on the pyridyl ring of the cyclometalating ligand results in a universal bathochromic shift of the phosphorescence of the iridium complexes. The phosphorescent lifetimes of complexes **Ir-1–Ir-5** are determined in the range of 1.77–2.18  $\mu\text{s}$  at room temperature. Relative to  $\text{Ir}(\text{ppy})_2(\text{acac})$  ( $\Phi_p = 0.34$ ) as the standard [36], the phosphorescent quantum yields of these were measured in degassed  $\text{CH}_2\text{Cl}_2$  and they all

**Table 1**  
Photophysical and electrochemical data for complexes **Ir-1–Ir-5**.

Compound	$\lambda_{\text{abs}}$ [nm] <sup>a</sup>	$\lambda_{\text{em}}$ [nm] <sup>b</sup>	$\Phi_p$ <sup>b</sup>	$\tau_p$ [ $\mu\text{s}$ ] <sup>c</sup>	$E_g$ [eV] <sup>d</sup>	$E_{\text{onset}}^{\text{ox}}$ [V]	HOMO/LUMO [eV] <sup>e</sup>	$\Delta T_{5\%}$ [°C]
<b>Ir-1</b>	259 (0.58), 293 (0.28), 345 (0.29), 444 (0.033)	517	0.18	1.92	2.45	0.83	−5.23/−2.78	378
<b>Ir-2</b>	257 (0.75), 294 (0.49), 345 (0.44), 445 (0.027)	513	0.19	1.78	2.51	0.79	−5.19/−2.68	385
<b>Ir-3</b>	257 (0.66), 294 (0.32), 335 (0.31), 445 (0.027)	519	0.27	1.77	2.41	0.81	−5.21/−2.80	388
<b>Ir-4</b>	257 (0.92), 284 (0.49), 345 (0.44), 444 (0.054)	518	0.14	1.84	2.44	0.94	−5.34/−2.90	367
<b>Ir-5</b>	260 (1.31), 290 (0.79), 369 (0.54), 478 (0.081)	543	0.31	2.18	2.26	0.88	−5.28/−3.02	382

<sup>a</sup> Measured in  $\text{CH}_2\text{Cl}_2$  with a concentration of  $10^{-5}$  M and  $\epsilon$  values ( $\times 10^5$ ) are shown in parentheses.

<sup>b</sup> In degassed  $\text{CH}_2\text{Cl}_2$ ,  $\Phi_p$  is shown relative to  $\text{fac}[\text{Ir}(\text{ppy})_3]$  ( $\Phi_p = 0.40$ ).

<sup>c</sup> Emission lifetime in degassed  $\text{CH}_2\text{Cl}_2$  with a concentration of  $10^{-5}$  M at 293 K,  $\lambda_{\text{exc}} = 410$  nm.

<sup>d</sup> Estimated from the absorption edge ( $\lambda_{\text{edge}}$ ) of solid films by equation of  $E_g = 1240/\lambda_{\text{edge}}$ .

<sup>e</sup> HOMO =  $-e(4.4 + E_{\text{onset}}^{\text{ox}})$ , LUMO = HOMO +  $E_g$ .

show high quantum efficiencies ranging from 0.14 to 0.31. Apparently, the phosphorescent efficiency of **Ir-5** is comparable with that of (ppy)<sub>2</sub>Ir(acac). The good electroluminescent behavior can be expected for these complexes based on the proper triplet energy levels and the high photoluminescent quantum yields.

### 3.3. Electrochemical characterization

The electrochemical properties of these new iridium complexes were measured in deoxygenated CH<sub>2</sub>Cl<sub>2</sub> solutions containing 0.1 M tetra(*n*-butyl)ammonium hexafluorophosphate (*n*-Bu<sub>4</sub>NPF<sub>6</sub>) as the supporting electrolyte by cyclic voltammetry. The cyclic voltammograms are shown in Fig. 3. During the anodic scan at the rate of 100 mV s<sup>-1</sup>, all these complexes show one reversible oxidation wave in the range of 0.79–0.94 V vs. a saturated calomel electrode (SCE), which should be assigned to the metal centered Ir<sup>III</sup>/Ir<sup>IV</sup> oxidation couple and/or the possible oxidation of the aryl part or the electron-donating carbazole group on the cyclometalating ligand. Compared to the complex (ppy)<sub>2</sub>Ir(acac) (0.72 V), the oxidation of these new iridium complexes become a little more difficult. It is found that introducing the electron-donating groups (4-CH<sub>3</sub>, 5-CH<sub>3</sub>) in the pyridine unit makes the oxidation process shift slightly to more positive potential for these complexes, while electron-withdrawing groups (5-F, 5-CF<sub>3</sub>) lead to less positive values. On the basis of the onset potential of the first oxidation ( $E_{\text{onset}}^{\text{ox}}$ ) and the absorption edge data, the HOMO and LUMO energy levels can be estimated from the empirical formulae:  $E_{\text{HOMO}} = -e(E_{\text{onset}}^{\text{ox}} + 4.4)$  and  $E_{\text{LUMO}} = E_{\text{HOMO}} + E_g$  (where  $E_g$  is the optical energy gap obtained from the absorption threshold of the film samples). All the electrochemical and electronic data for these novel iridium complexes are summarized in Table 1. For complex **Ir-1**, both the HOMO and LUMO decreased relative to those of the parent (ppy)<sub>2</sub>Ir(acac). However, the larger downwards shift of the LUMO than HOMO similarly leads to a smaller HOMO–LUMO band gap in comparison with the (ppy)<sub>2</sub>Ir(acac). A small decrease of 0.24 eV of the LUMO level was detected for **Ir-5** in comparison with **Ir-1**, in combination with the unchanged HOMO level, finally resulting in a similar decrease of the HOMO–LUMO band gap due to incorporation of the 5-CF<sub>3</sub> substituent.

In order to understand the impact of the modification groups (–CH<sub>3</sub>, –F and –CF<sub>3</sub>) on the photophysical and electrochemical behavior of these iridium complexes, density functional theory (DFT) calculations were performed for complexes **Ir-1**–**Ir-5** using

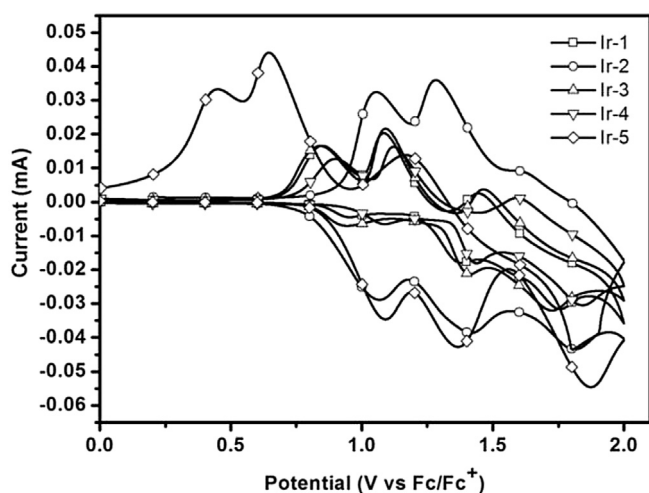


Fig. 3. Cyclic voltammograms of **Ir-1**–**Ir-5** measured in CH<sub>2</sub>Cl<sub>2</sub> at a scan rate of 100 mV s<sup>-1</sup>.

B3LYP hybrid functional theory with Gaussian 09. Fig. 4 illustrates the HOMO and LUMO distributions for complexes **Ir-1** and **Ir-5**. Those for **Ir-2**, **Ir-3** and **Ir-4** are provided in Fig. S1 in the Supporting Information. For all present complexes, the HOMOs are localized on the iridium center and the phenyl and carbazole of the cyclometalating ligands as described in the literature. On the other hand, the LUMO orbitals of these iridium(III) complexes are distributed on both the aryl and pyridyl rings of the cyclometalating ligands. It was noteworthy that **Ir-5** with the 5-CF<sub>3</sub> on the pyridyl ring, the LUMO of the novel complex is more intensively shifted onto the pyridyl ring in comparison with **Ir-1**. The shifting of the LUMO distribution and the lower levels are probably because that the strong electron-withdrawing –CF<sub>3</sub> substituent further enhances the electron-deficient feature of the pyridyl moiety.

### 3.4. Electrophosphorescent OLEDs

In order to investigate the EL properties of these iridium complexes, **Ir-1** and **Ir-5** were used as doped emitters to fabricate monochromatic OLEDs, as shown in Fig. 5. From the high energy band of the phosphorescence spectra, the triplet energies were determined as ca. 2.26–2.47 eV for **Ir-1**–**Ir-5**. These energy levels are well below the level of the widely used CBP (2.56 eV) host and the efficient energy transfer process is possible if CBP is selected as the host matrix for these complexes to fabricate OLEDs. Two types of light-emitting devices were fabricated using **Ir-1** or **Ir-5** as phosphorescent emitters. The device structures are as follows: ITO/NPB (40 nm)/CBP: iridium complex (6%, 30 nm)/TPBI (45 nm)/LiF (1 nm)/Al (device **I**), and ITO/NPB (40 nm)/TCTA (10 nm)/CBP: iridium complex (6%, 30 nm)/TPBI (45 nm)/LiF (1 nm)/Al (device **II**), where NPB was used as the hole-transporting layer, TCTA (4,4',4''-tris(carbazol-9-yl)-triphenylamine) as the electron/exciton-blocking layer, CBP as the host material and TPBI as an electron-transporting/hole-blocking material. Different hole-transporting layers were utilized for these two devices in order to verify their influence on the device performances.

As an example, the EL spectra of **Ir-1** in device **I** and its PL at room temperature and at 77 K are illustrated in Fig. 6. The EL spectrum of **Ir-1** is consistent with the PL spectrum at room temperature and indicates that the EL originates from the triplet states of the phosphor. Typical of other similar iridium complexes, the spectra experience a blue-shift of about 16 nm in glass matrices at 77 K as a consequence of rigidification. This blue-shift is a frequently observed phenomenon and is mainly due to the solvent reorganization in a fluid solution at low temperature that can

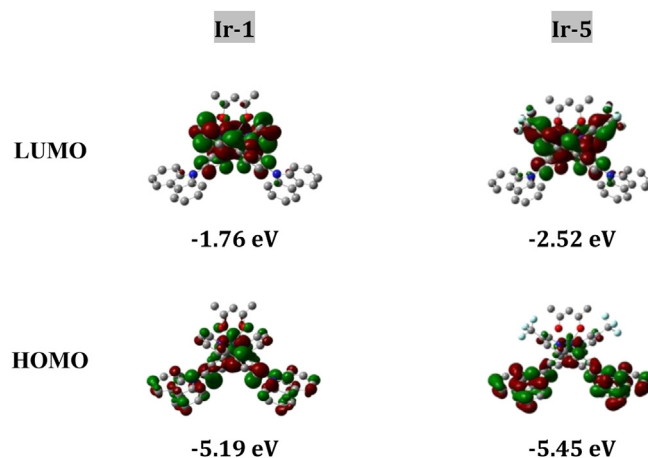


Fig. 4. Contour plots of frontier molecular orbitals of **Ir-1** and **Ir-5** in ground state.

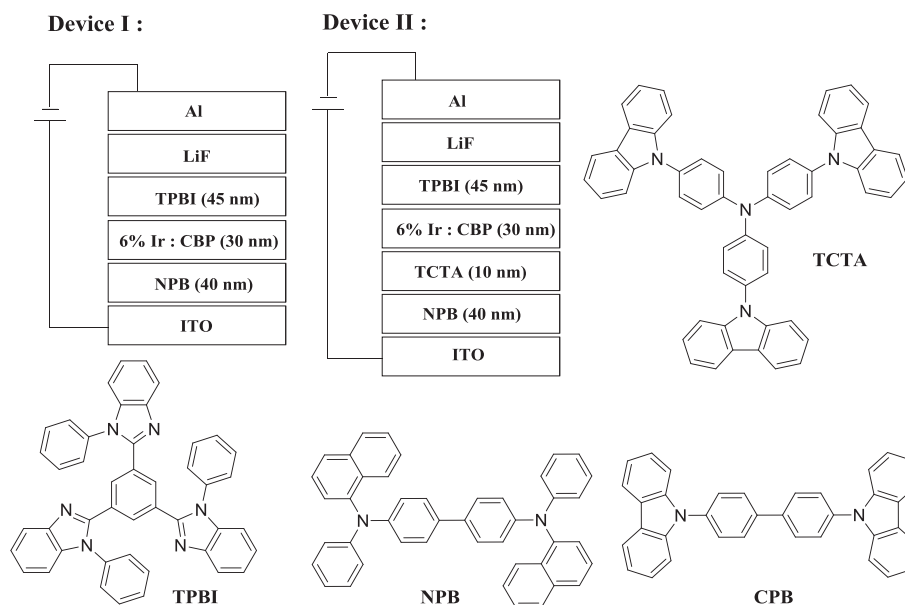


Fig. 5. The general structure for OLED devices and the molecular structures of the relevant.

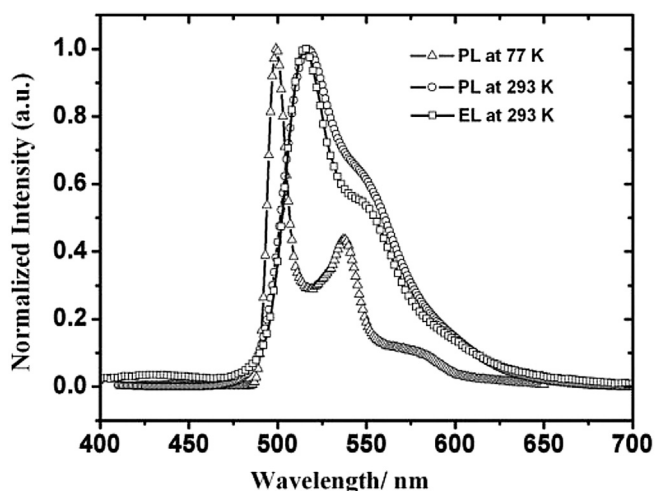


Fig. 6. The PL and EL spectra for Ir-1.

stabilize the charge transfer states prior to emission [37]. No residual emission from CBP or TPBI is observed, which suggests an efficient energy transfer from the host exciton to the phosphor molecule upon electrical excitation and the effective hole-blocking function of the TPBI layer in addition to its electron-transporting role. The EL performance data of Ir-1 and Ir-5 in different devices are listed in Table 2. In devices I and II, both complexes exhibited excellent device performances. For example, the performance of

Table 2  
EL data of the different OLED devices based on Ir-1 and Ir-5.

Complex	$V_{\text{turn-on}}$ [V]	$L_{\text{max}}$ [cd m <sup>-2</sup> , V] <sup>a</sup>	$\eta_{\text{ext}}$ [% , V] <sup>a</sup>	$\eta_L$ [cd A <sup>-1</sup> , V] <sup>a</sup>	$\eta_P$ [lm W <sup>-1</sup> , V] <sup>a</sup>	$\lambda_{\text{em}}$ [nm]	CIE (x, y) at 9 V
Ir-1 (I)	4.7	38,400, 10	10.7, 5	36.7, 5	19.2, 5	516	0.28, 0.62
Ir-5 (I)	4.5	56,140, 14	11.0, 6	39.1, 6	24.5, 6	542	0.40, 0.56
Ir-1 (II)	4.4	45,650, 10	11.4, 5	40.7, 5	25.5, 5	516	0.27, 0.61
Ir-5 (II)	4.2	30,430, 11	12.6, 5	43.2, 5	27.1, 5	543	0.40, 0.56

<sup>a</sup> The maximum values of the devices. The data in the parentheses are the voltages (V) at which the data are obtained.

the Ir-1-based device I is quite remarkable with a high luminance of 56,140 cd m<sup>-2</sup> at 14 V and a peak luminance efficiency ( $\eta_L$ ) of 36.7 cd A<sup>-1</sup>, corresponding to a peak power efficiency ( $\eta_P$ ) of 19.2 lm W<sup>-1</sup>. As illustrated by the efficiency-current density curves in Fig. 7, both of the devices witness gradual efficiency decay at the

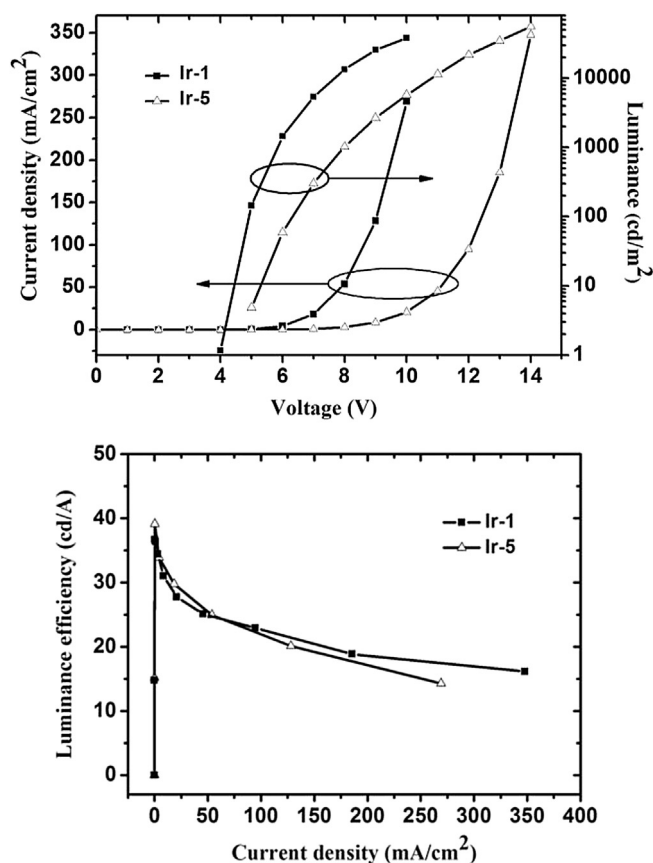


Fig. 7. J–V–L characteristics and current efficiency–current density curves for Ir-1 and Ir-5 in device I.

higher current density region, which are typically attributed to a combination of triplet–triplet annihilation and field-induced quenching effects.

By introducing TCTA as the electron/exciton-blocking layer, the current density over the whole detected voltage range is always higher in device **II** than in device **I** for each complex, as indicated by the data under an example voltage of 9 V (Table 2). The better performance for device **II** should be resulting from a more balanced electron and hole transportation and more efficient recombination in the emitting layer that is brought by using TCTA as the electron/exciton-blocking layer. As a result, the device **II** exhibits overall improvements in the turn-on voltage, brightness, and EL efficiencies. For example, the turn-on voltages of device **II** are 4.2–4.4 V, which are lower than 4.5–4.7 V for device **I**. The decreased driving voltages in device **II** will be definitely favorable to higher power efficiencies, as shown by the efficiency–current density curves in Fig. 8 and the data in Table 2. The performance of **Ir-1** and **Ir-5** in device **II** is substantially enhanced, with peak  $\eta_L = 40.7 \text{ cd A}^{-1}$  and  $\eta_P = 25.5 \text{ lm W}^{-1}$  for **Ir-1** and  $\eta_L = 43.2 \text{ cd A}^{-1}$  and  $\eta_P = 27.1 \text{ lm W}^{-1}$  for **Ir-5**. We particularly note that the overall performances of **Ir-5** are better than **Ir-1** in both devices **I** and **II**, with lower driving voltages and higher luminance and especially remarkably higher efficiencies. The introduction of the electron-withdrawing  $-\text{CF}_3$  group contributes to the outstanding OLEDs performance. As reported in the literature, fluorination can enhance the electron mobility and result in a better balance of charge injection and transfer. In addition, the lower vibrational frequency of the C–F may reduce the rate of radiationless deactivation [38,39].

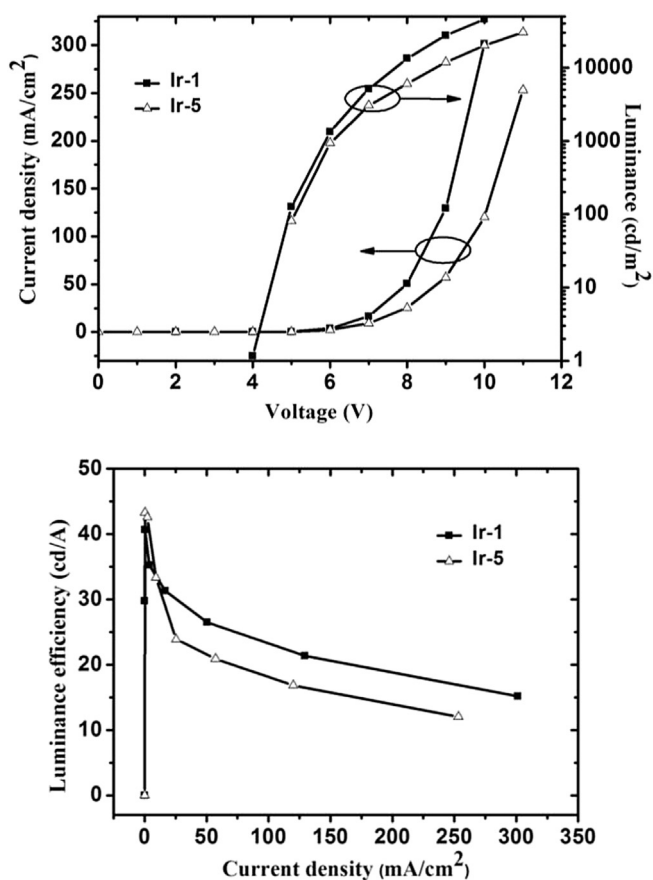


Fig. 8.  $J$ – $V$ – $L$  characteristics and current efficiency–current density curves for **Ir-1** and **Ir-5** in device **II**.

In recent years, white organic light-emitting diodes have been of considerable interest due to their potential applications in solid-state lighting and full-color displays. For display applications, it is important that the generated white light can be separated into three primary colors with equal emission intensity after passing through the color filters [40,41]. Chen et al. reported that in order to generate the white spectrum with three evenly separated red, green and blue peaks, the central emission wavelength of the green emitter should be located at 545 nm [42]. We particularly note that in this work the complex **Ir-5** is easily synthesized as a new yellowish-green emitter, with a central electroluminescence wavelength of 543 nm. We also expect that the EL performance of **Ir-5** could be further optimized by choosing other novel host materials.

#### 4. Conclusions

In conclusion, a series of heteroleptic cyclometalated iridium(III) complexes containing 9-(4-(pyridin-2-yl)phenyl)-9H-carbazole molecular framework have been synthesized and fully characterized. All of the complexes are thermally stable solids and highly efficient electrophosphors. This work presents a systematic investigation of the substituent effects on the luminescent properties of (ppy-carbazole)<sub>2</sub>Ir(acac) derivatives. It is noteworthy that **Ir-5** is an excellent green–yellow phosphorescent material with a maximum luminance efficiency of  $43.2 \text{ cd A}^{-1}$  and a power efficiency of  $27.1 \text{ lm W}^{-1}$ , which has potential applications in white OLEDs.

#### Acknowledgment

Financial support by the National Natural Science Foundation of China (21276043) and the Ministry of Education (the Program for New Century Excellent Talents in University NCET-10-0283) is acknowledged. We thank Dr. Jiuyan Li (Dalian University of Technology) for OLEDs measurements.

#### Appendix A. Supplementary data

Supplementary data related to this article can be found at <http://dx.doi.org/10.1016/j.dyepig.2014.04.039>.

#### References

- [1] Tang C, VanSlyke S. Organic electroluminescent diodes. *Appl Phys Lett* 1987;51:913.
- [2] Kido J, Kimura M, Nagai K. Multilayer white light-emitting organic electroluminescent device. *Science* 1995;267(5202):1332–4.
- [3] Xiao L, Chen Z, Qu B, Luo J, Kong S, Gong Q, et al. Recent progresses on materials for electrophosphorescent organic light-emitting devices. *Adv Mater* 2011;23(8):926–52.
- [4] Baldo M, O'Brien D, You Y, Shoustikov A, Sibley S, Thompson M, et al. Highly efficient phosphorescent emission from organic electroluminescent devices. *Nature* 1998;395(6698):151–4.
- [5] Dias HVR, Diyabalanage HVK, Eldabaja MG, Elbjairami O, Rawashdeh-Omary MA, Omary MA. Brightly phosphorescent trinuclear copper(I) complexes of pyrazolates: substituent effects on the supramolecular structure and photophysics. *J Am Chem Soc* 2005;127:7489–501.
- [6] Rudmann H, Shimada S, Rubner MF. Solid-state light-emitting devices based on the tris-chelated ruthenium (II) complex. 4. High-efficiency light-emitting devices based on derivatives of the tris(2, 2'-bipyridyl) ruthenium(II) complex. *J Am Chem Soc* 2002;124(17):4918–21.
- [7] Tung Y-L, Wu P-C, Liu C-S, Chi Y, Yu J-K, Hu Y-H, et al. Highly efficient red phosphorescent osmium(II) complexes for OLED applications. *Organometallics* 2004;23(15):3745–8.
- [8] Kwong RC, Sibley S, Dubovoy T, Baldo M, Forrest SR, Thompson ME. Efficient, saturated red organic light emitting devices based on phosphorescent platinum(II) porphyrins. *Chem Mater* 1999;11(12):3709–13.
- [9] King KA, Spellane PJ, Watts RJ. Excited-state properties of a triply orthometalated iridium(III) complex. *J Am Chem Soc* 1985;107(5):1431–2.
- [10] Chen ZQ, Bian ZQ, Huang CH. Functional Ir(III) complexes and their applications. *Adv Mater* 2010;22(13):1534–9.

- [11] Ulbricht C, Beyer B, Friebe C, Winter A, Schubert US. Recent developments in the application of phosphorescent iridium(III) complex systems. *Adv Mater* 2009;21(44):4418–41.
- [12] You Y, Park SY. Inter-ligand energy transfer and related emission change in the cyclometalated heteroleptic iridium complex: facile and efficient color tuning over the whole visible range by the ancillary ligand structure. *J Am Chem Soc* 2005;127(36):12438–9.
- [13] Li J, Djurovich PI, Alleyne BD, Yousufuddin M, Ho NN, Thomas JC, et al. Synthetic control of excited-state properties in cyclometalated Ir(III) complexes using ancillary ligands. *Inorg Chem* 2005;44(6):1713–27.
- [14] Ho CL, Wang Q, Lam CS, Wong WY, Ma D, Wang L, et al. Phosphorescence color tuning by ligand, and substituent effects of multifunctional iridium(III) cyclometalates with 9-arylcarbazole moieties. *Chem Asian J* 2009;4(1):89–103.
- [15] Ikawa S, Yagi S, Maeda T, Nakazumi H, Fujiwara H, Sakurai Y. Photoluminescence color tuning of phosphorescent bis-cyclometalated iridium(III) complexes by ancillary ligand replacement. *Dyes Pigments* 2012;95(3):695–705.
- [16] Hwang F-M, Chen H-Y, Chen P-S, Liu C-S, Chi Y, Shu C-F, et al. Iridium(III) complexes with orthometalated quinoxaline ligands: subtle tuning of emission to the saturated red color. *Inorg Chem* 2005;44(5):1344–53.
- [17] Beeby A, Bettington S, Samuel IDW, Wang Z. Tuning the emission of cyclometalated iridium complexes by simple ligand modification. *J Mater Chem* 2003;13(1):80–3.
- [18] Tsuzuki T, Shirasawa N, Suzuki T, Tokito S. Color tunable organic light-emitting diodes using pentafluorophenyl-substituted iridium complexes. *Adv Mater* 2003;15(17):1455–8.
- [19] Wang R, Liu D, Ren H, Zhang T, Yin H, Liu G, et al. Highly efficient orange and white organic light-emitting diodes based on new orange iridium complexes. *Adv Mater* 2011;23(25):2823–7.
- [20] Avilov I, Minoofar P, Cornil J, Cola LD. Influence of substituents on the energy and nature of the lowest excited states of heteroleptic phosphorescent Ir(III) complexes: a joint theoretical and experimental study. *J Am Chem Soc* 2007;129(26):8247–58.
- [21] Tang H, Li Y, Wei C, Chen B, Yang W, Wu H, et al. Novel yellow phosphorescent iridium complexes containing a carbazole-oxadiazole unit used in polymeric light-emitting diodes. *Dyes Pigments* 2011;91(3):413–21.
- [22] Adachi C, Baldo MA, Thompson ME, Forrest SR. Nearly 100% internal phosphorescence efficiency in an organic light-emitting device. *J Appl Phys* 2001;90(10):5048–51.
- [23] Tsuzuki T, Tokito S. Highly efficient and low-voltage phosphorescent organic light-emitting diodes using an iridium complex as the host material. *Adv Mater* 2007;19(2):276–80.
- [24] Bettington S, Tavasli M, Bryce MR, Beeby A, Al-Attar H, Monkman AP. Tris-cyclometalated iridium(III) complexes of carbazole(flourenyl)pyridine ligands: synthesis, redox and photophysical properties, and electrophosphorescent light-emitting diodes. *Chem Eur J* 2007;13(5):1423–31.
- [25] Ho C-L, Chi L-C, Hung W-Y, Chen W-J, Lin Y-C, Wu H, et al. Carbazole-based coplanar molecule (CmInF) as a universal host for multi-color electrophosphorescent devices. *J Mater Chem* 2012;22(1):215–24.
- [26] Yang C, Zhang X, You H, Zhu L, Chen L, Zhu L, et al. Tuning the energy level and photophysical and electroluminescent properties of heavy metal complexes by controlling the ligation of the metal with the carbon of the carbazole unit. *Adv Funct Mater* 2007;17(4):651–61.
- [27] Liu D, Yang R, Wang R. Highly efficient orange and white electrophosphorescence from solution-processible iridium(III) complexes. *Dyes Pigments* 2013;98(3):317–22.
- [28] Mei Q, Wang L, Tian B, Tong B, Weng J, Zhang B, et al. Highly efficient red iridium(III) complexes based on phthalazine derivatives for organic light-emitting diodes. *Dyes Pigments* 2012;97(1):43–51.
- [29] Rao X, Liu C, Qiu J, Jin Z. A highly efficient and aerobic protocol for the synthesis of N-heteroaryl substituted 9-arylcarbazolyl derivatives via a palladium-catalyzed ligand-free Suzuki reaction. *Org Biomol Chem* 2012;10(39):7875–83.
- [30] Brunner K, van Dijken A, Börner H, Bastiaansen JJ, Kiggen NM, Langeveld BM. Carbazole compounds as host materials for triplet emitters in organic light-emitting diodes: tuning the HOMO level without influencing the triplet energy in small molecules. *J Am Chem Soc* 2004;126(19):6035–42.
- [31] Tao Y, Wang Q, Yang C, Wang Q, Zhang Z, Zou T, et al. A simple carbazole/oxadiazole hybrid molecule: an excellent bipolar host for green and red phosphorescent OLEDs. *Angew Chem Int Ed* 2008;120(42):8224–7.
- [32] You J, Li G, Wang R, Nie Q, Wang Z, Li J. Pyrene-cored dendrimer with carbazole derivatives as dendrons: synthesis, properties and application in white light-emitting diode. *Phys Chem Chem Phys* 2011;13(39):17825–30.
- [33] Ono K, Joho M, Saito K, Tomura M, Matsushita Y, Naka S, et al. Synthesis and electroluminescence properties of fac-tris(2-phenylpyridine)iridium derivatives containing hole-trapping moieties. *Eur J Inorg Chem* 2006;18:3676–83.
- [34] Ho C-L, Wong W-Y, Yao B, Xie Z, Wang L, Lin Z. Synthesis, characterization, photophysics and electrophosphorescent applications of phosphorescent platinum cyclometalated complexes with 9-arylcarbazole moieties. *J Organomet Chem* 2009;694(17):2735–49.
- [35] Lamansky S, Djurovich P, Murphy D, Abdel-Razzaq F, Kwong R, Tsyba I, et al. Synthesis and characterization of phosphorescent cyclometalated iridium complexes. *Inorg Chem* 2001;40:1704–11.
- [36] Tamayo AB, Alleyne BD, Djurovich PI, Lamansky S, Tsyba I, Ho NN, et al. Synthesis and characterization of facial and meridional tris-cyclometalated iridium(III) complexes. *J Am Chem Soc* 2003;125(24):7377–87.
- [37] Zhou G, Ho C-L, Wong W-Y, Wang Q, Ma D, Wang L, et al. Manipulating charge-transfer character with electron-withdrawing main-group moieties for the color tuning of iridium electrophosphors. *Adv Funct Mater* 2008;18(3):499–511.
- [38] Li H-Y, Zhou L, Teng M-Y, Xu Q-L, Lin C, Zheng Y-X, et al. Highly efficient green phosphorescent OLEDs based on a novel iridium complex. *J Mater Chem C* 2013;1(3):560–5.
- [39] Xu QL, Wang CC, Li TY, Teng MY, Zhang S, Jing YM, et al. Syntheses, photoluminescence, and electroluminescence of a series of iridium complexes with trifluoromethyl-substituted 2-phenylpyridine as the main ligands and tetraphenylimidodiphosphate as the ancillary ligand. *Inorg Chem* 2013;52(9):4916–25.
- [40] Kamtekar KT, Monkman AP, Bryce MR. Recent advances in white organic light-emitting materials and devices (WOLEDs). *Adv Mater* 2010;22(5):572–82.
- [41] Farinola GM, Ragni R. Electroluminescent materials for white organic light emitting diodes. *Chem Soc Rev* 2011;40(7):3467–82.
- [42] Chen S, Tan G, Wong WY, Kwok HS. White organic light-emitting diodes with evenly separated red, green, and blue colors for efficiency/color-rendition trade-off optimization. *Adv Funct Mater* 2011;21(19):3785–93.